# Behavior of high-order stimulated Raman scattering in a highly transient regime

Emiliano Sali,* Paul Kinsler, G. H. C. New, K. J. Mendham, Thomas Halfmann,† J. W. G. Tisch, and J. P. Marangos
*Blackett Laboratory, Imperial College London, London SW7 2BW, United Kingdom*
(Received 15 October 2004; published 18 July 2005)

We have investigated the behavior of high-order stimulated Raman scattering in a highly-transient regime. We demonstrate efficient collinear generation of vibrational sidebands in molecular hydrogen and methane using two-color pumping with pulses of duration $\tau \sim 100$ fs tuned to a vibrational Raman transition. A Raman spectrum with a large bandwidth was observed, ranging from the IR to the UV. Under some conditions strong pump depletion was observed and up to five anti-Stokes sidebands were observed to have energies exceeding 10% of the transmitted pump pulse energies. A numerical simulation reproduces qualitatively and quantitatively the experimental results and allows us to explain key experimental features. The simulation also confirms that the molecular coherence in the medium is substantially increased by the two-color pumping and allows us to deduce values for the degree of material excitation. The use of this technique looks promising for efficient subfemtosecond pulse generation.

DOI: 10.1103/PhysRevA.72.013813 PACS number(s): 42.65.Dr, 42.50.Gy, 42.65.Re, 42.65.Jx

## I. INTRODUCTION

At present the shortest ultrafast light pulses are achieved using extreme-ultraviolet (XUV) and x-ray radiation and enter the subfemtosecond or *attosecond* regime (1 as $=10^{-18}$ s) [1–3]. *High-order stimulated Raman scattering* (HSRS) holds the potential to generate ultrabroadband light pulses with an energy conversion efficiency approaching unity [4,5]. On the other hand, attosecond pulses generated using high-harmonic generation (HHG) have very low energy, as a consequence of the intrinsic low conversion efficiency of the process ($\sim 10^{-6}$). HSRS can be considered as an interesting alternative to HHG, as it has the potential to produce pulses that are still potentially in the sub-fs regime but much more energetic (by a factor of $\sim 10^4$) than those obtained through HHG.

This paper describes an experimental and numerical investigation of high-order stimulated Raman scattering (HSRS) in a highly-transient regime carried out using two $\sim 100$ fs laser pulses of comparable energy tuned to Raman resonance with a vibrational transition in molecular gases. We report on numerical modelling carried out in order to reproduce the experimental results and to gain a deeper understanding of the underlying physical mechanisms.

Recently the potential for high efficiency broad-band HSRS production using this method was demonstrated experimentally [6]. In that work, the first pulse was provided by a Ti:sapphire chirped-pulse amplified (CPA) laser system, whereas the second pump pulse was obtained from a frequency-tunable optical parametric amplifier (OPA) pumped by a fraction of the same Ti:sapphire laser. Very broadband Raman spectra were generated at the output. Depending on the experimental parameters, these spectra could consist of either discrete sidebands or very broad *supercontinua*. The numerical model provides good qualitative agreement with the results which allows us to deduce values for the degree of material excitation. With the aid of this model we can make explicit predictions about the spatio-temporal evolution of the coherence, from which we predict an alternative scheme for high efficiency Raman side-bands generation from a delayed pulse. Also, further experimental studies are reported (compared to Ref. [6]) on the dependence of the HSRS process upon molecular species, density, and laser properties (intensity, pulse duration, and polarization). We measured the dependence of the spectrum shapes on pressure in hydrogen and methane, and we can explain the differences between the broadening in the two cases. Also, we quantified how the supercontinuum formation can be controlled by means of a slight stretching of the pump pulse duration. These results are discussed in detail and give new insight into the physical nature of the process.

In HSRS a key role is played by the temporal duration of the driving pulses. The relevant characteristic time constant is the *dephasing time* $T_2$ of the molecular oscillations (rotations or vibrations). The ratio between the pump pulse duration and the dephasing time $T_2$ defines the different regimes of HSRS [7]. In the *quasistationary* regime the duration of the pump laser pulses is significantly longer than $T_2$, whereas in the *transient* regime the laser pulse duration is comparable to or shorter than $T_2$. It needs to be pointed out here that the terms *quasistationary* and *transient* are referred only to the pulse duration and not to the excitation of the molecular medium, which is "transient" in the quasistationary case too, in the sense that it exists only when the pulses are present and it decays afterwards on the much faster timescale of the dephasing time.

If the pulse duration is even shorter than the characteristic period of the molecular motion (i.e., the vibrational period $T_v$), the *impulsive* regime is entered [8]. Reaching the impulsive regime for many molecular vibrational modes of interest requires laser pulse durations of a few tens of femtoseconds

*Present address: European Laboratory for Nonlinear Spectroscopy (LENS), Via Nello Carrara 1, I-50019 Sesto Fiorentino (FI), Italy. Electronic address: sali@lens.unifi.it.

†Present address: Department of Physics, Technical University of Kaiserslautern, Germany.

 

or even shorter, depending on the frequency of the relevant molecular oscillation.

As we used laser pulses with a duration of the order of ~100 fs, our experiments are well into the transient regime. Reaching the impulsive regime requires pump pulses shorter than 10 fs for the molecular systems considered here. Typical values of $T_2$ for molecular systems at the relevant densities (0.1–1 bar) range from a few hundred picoseconds to a few nanoseconds. Therefore, the case of the quasistationary regime corresponds to pump pulses of nanosecond duration or longer, whereas the transient regime is reached for shorter pulse durations. In our experiments we used hydrogen and methane ($H_2$ and $CH_4$), whose dephasing times $T_2$ at pressure $P=10^5$ Pa are ~2.6 ns and ~30 ps, respectively.

Sokolov *et al.* experimentally demonstrated the generation of HSRS sidebands with high conversion efficiency in the quasistationary regime using a pair of nanosecond pump pulses tuned to a vibrational Raman resonance in deuterium [9] and a rotational Raman resonance in hydrogen [10]. The compression of the generated spectra to a train of pulses with a duration $\tau \sim 2$ fs has been demonstrated by phase-controlled multi-photon ionization in xenon, where the phases of different generated sidebands were manipulated externally [11].

An *adiabatic* evolution of the quantum system is essential in the HSRS scheme of Sokolov *et al.*, in order to efficiently prepare a coherent superposition of the ground and first excited state. To achieve that, in the quoted experiments of Sokolov *et al.* a pair of pulses with a duration of $\tau \sim 10$ ns were used to prepare the medium with a large value of vibrational coherence. Since the vibrational period of deuterium is only 10 fs this results in the generation of a train of $\sim 10^6$ pulses. This means that the energy in each pulse of the train is very low, which is not convenient for many applications.

When ultrashort pulses are used the number of pulses in the train can be substantially reduced, but at the same time the efficiency of the Raman conversion process is reduced with respect to the quasistationary case due to competing nonlinear effects such as self-phase modulation or self-focusing.

Nevertheless, it has been demonstrated that coherent molecular oscillations can be efficiently produced in the impulsive regime [5], using one pump pulse with a duration shorter than the vibrational period of the molecular medium. In the frequency domain this corresponds to a pump pulse with a bandwidth exceeding the frequency difference between the two Raman levels [12], which means that the pump pulse contains pairs of Raman-resonant frequency components within the pulse bandwidth (Fig. 1). After the pump pulse has passed, a wave of vibrational excitations propagates in the medium with a velocity equal to the group velocity of the pump pulse. The lifetime of this excitation is determined by the dephasing time, which is longer than the pulse duration. A weaker delayed probe pulse experiences phase modulation in a linear regime [13] upon propagation in the coherently prepared medium, leading to the generation of a comb of sidebands.

For molecules with large vibrational frequencies, this scheme cannot be implemented using lasers delivering pulses with a duration of $\tau \gtrsim 50$ fs, since this pulse duration is too long to meet the impulsive condition. To satisfy the impulsive condition, either a Raman medium with a relatively long oscillation period or a pump laser with a few-cycle pulse duration must be used. The latter condition is required if one wants to excite a very high-frequency oscillation, like a vibrational motion in hydrogen, whose period is approximately 10 fs. This scheme is therefore impossible to implement in many cases using a conventional Ti:sapphire laser.

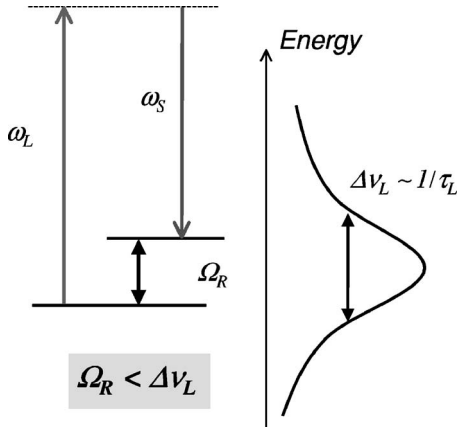


FIG. 1. Stimulated Raman scattering in the impulsive regime. The laser pulse bandwidth is larger than the frequency spacing of the Raman transition, therefore the pulse contains pairs of Raman-resonant frequency components ($\omega_L$ and $\omega_s$).

When pump pulses with temporal duration in the $\tau \gtrsim 50$ fs regime are used (as is the case for most of the conventional Ti:sapphire laser systems) one can speak of a *highly-transient* regime, since the laser pulse duration is much shorter than the dephasing time $T_2$ of the molecular vibrations, but it is still longer than the vibrational period of most of the Raman-active molecules (Fig. 2), in our case by a factor of ~10. Under these conditions, competing nonlinear effects, which are mostly detrimental when the Raman

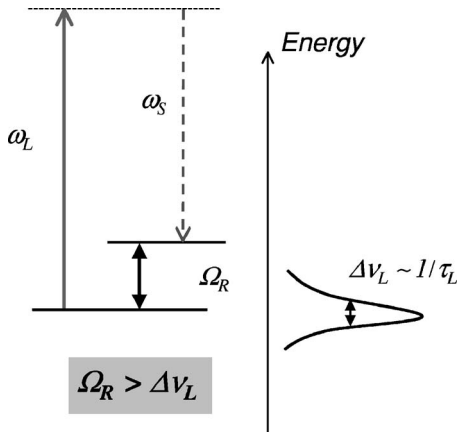


FIG. 2. Stimulated Raman scattering in a highly-transient regime with one pump pulse. The laser pulse bandwidth is smaller than the frequency spacing of the Raman transition, therefore the Stokes frequency $\omega_s$ must grow from noise through spontaneous Raman scattering pumped by $\omega_L$. This is not required if *two* Raman-resonant pump pulses are used instead.

gain is low [14], can effectively prevent the Raman process from taking place efficiently. Most of the experiments on transient HSRS in gases reported in the literature have been carried out using only one pump laser [15,16]. In these cases the first Stokes sideband must grow from the background noise before efficient generation of high-order sidebands can occur.

The efficiency of the process can be considerably increased if a second pump field with comparable pulse duration and energy is applied and the frequencies of both lasers are tuned to a Raman resonance [17–19]. This can be explained by the fact that the HSRS process can be viewed as the combination of a SRS process to produce a Stokes sideband followed by parametric four-wave Raman mixing, which produces higher-order Stokes and anti-Stokes Raman sidebands [7]. In this "two-color" configuration one does not need to wait for the first Stokes sideband to be generated in order for the higher-order sidebands generation to take place. One experiment of this kind carried out in solid $KGd(WO_4)_2$ is reported in the literature [20] but no experiments using gases had been reported before Ref. [6].

In the next sections the details of this experimental and numerical investigation are described. The structure of the manuscript is as follows: Sec. II outlines the theory behind the process and the numerical model and the details of how the calculation is implemented and which approximations are made. Section III describes the experimental setup. In Sec. IV the complete set of experimental results is presented; this include previously unpublished results on the polarization-dependence of the HSRS spectra as well as a significantly more detailed set of experimental results (compared to those reported in Ref. [6]) for the dependence of the Raman spectra upon gas species, pump pulse duration and pressure. Section V presents the results of the numerical simulation and a comparison with the experimental results. Finally, Secs. VI and VII contain a discussion of the main results and the conclusions of this study.

## II. THEORY AND NUMERICAL MODEL

In order to gain a deeper understanding of the experimental results, a numerical model of the experiment was used. When driven strongly, a two-photon Raman transition modulates the incoming field by adding sidebands separated by the transition frequency—these sidebands then get modulated to generate sidebands of their own (and so on), thus producing the wide comb of frequency components separated by the Raman transition frequency. In standard treatments of the Raman process (e.g., Refs. [21,22]), the field is split up into frequency components centered on the teeth of the frequency comb. The approach has the advantage that the components can be modelled reasonably well with slowly varying envelopes, but of course it has the disadvantage of needing to keep track of a large number of components (an alternative strategy is suggested in [23]).

We use the standard semiclassical framework of the Bloch model, where the Raman transition is treated quantum mechanically as a two-level system, but the electric field is treated classically. The field is split into components which have frequencies ($\omega_i$) at integer spacings of the transition frequency ($\omega_b$) from the main pump laser frequency ($\omega_0$), with each component described using an envelope and carrier approach, allowing us to easily simulate propagating optical pulses. The field is therefore

$$E(t) = \sum_j [A_j(t)e^{i(k_j z-\omega_j t)} + A_j^*(t)e^{i(k_j z-\omega_j t)}], \tag{1}$$

where $k_j$ are the wave vectors of the $j$th field components. The Bloch vector of the Raman transition is driven by each combination of spectrally adjacent field components,

$$\frac{d\rho'_{12}}{dt} \approx \left(-\gamma_2 + ig\sum_j 2A_j^* A_j\right)\rho'_{12} + 2if\sum_j 2A_j A_{j-1}^* \,.\, w \,.\, e^{+i(k_j-k_{j-1})z}, \tag{2}$$

$$\frac{dw}{dt} = -\gamma_1(w-w_i) + 2if'(2A_j^* A_{j+1} \,.\, \rho'_{12}e^{i\omega_b t} - 2A_j A_{j+1}^* \,.\, \rho'^*_{12}e^{-i\omega_b t}), \tag{3}$$

where the Raman polarization is $\rho'_{12}=(u+iv)/2$, the inversion is $w$, the Raman coupling parameter is $f$, and the Stark shift parameter is $g$. Then, in turn, each of the field components $A_j$ is driven by the atomic polarization in combination with its adjacent field components $A_{j+1}$ and $A_{j-1}$; consequently they evolve as they propagate forward in $z$ according to

$$\frac{d}{dz}A_j(t) = i\frac{\sigma\hbar\omega_j f}{\epsilon_0 c_0}\{\rho'_{12}A_{j+1}\exp(+i(k_{j+1}-k_j)z) + \rho'^*_{12}A_{j-1}\exp(+i(k_{j-1}-k_j)z)\}, \tag{4}$$

where $\sigma$ is the density of the Raman medium.

A Cauchy dispersion model is also applied to the propagation of the field components, using the standard split-step method, where the (Raman) nonlinear effects and the dispersion are applied alternately. This has the advantage that the dispersion can be calculated in the frequency domain, which is considerably more efficient—in contrast to the Raman response, which is most efficiently solved in the time domain.

To avoid too much complexity, $\chi^{(3)}$ effects such as four-wave mixing and self-phase modulation are not taken into account. We will see later that this approximation still gives good agreement with the experimental results. Parameters related to the field-atom coupling (i.e., the Raman gain per unit length) are estimated using values obtained from the literature for our specific case.

## III. EXPERIMENTAL SETUP

The experimental setup is shown in Fig. 3. The output of the Ti:sapphire CPA system (central wavelength $\lambda_1 = 800$ nm, pulse duration $\tau_1 = 70$ fs, pulse energy $E = 20$ mJ, and repetition rate of 10 Hz) was divided by a beamsplitter. A small fraction of the pulse energy ($\sim 10\%$) was used to provide the first pump laser pulse at $\lambda_1 = 800$ nm. The largest

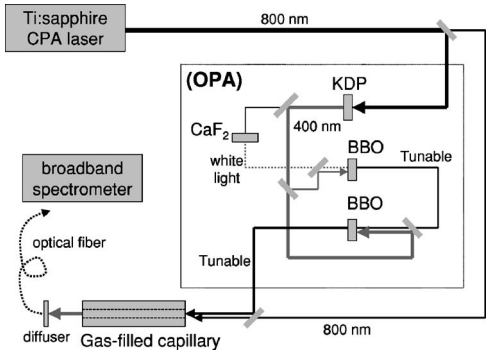


FIG. 3. Layout of the two-color stimulated Raman scattering experiment.

part ($\sim$90%) of the CPA pulse was frequency-doubled to provide the pump pulse for an optical parametric amplifier (OPA), which in turn provided the second pump pulse for the HRSR experiment.

The OPA was a double-stage collinear optical parametric amplifier seeded by white-light. The white-light seed was produced in a calcium-fluoride plate onto which was focused a small fraction of the infrared radiation which is not frequency-doubled in the KDP. The seed was subsequently amplified in two 2-mm-thick type-I BBO crystals. The output wavelength $\lambda_2$ was tunable from 450 to 800 nm and the pulse duration was estimated to be $\tau_2 \sim 250$ fs from dispersion calculations.

The Raman-active molecular medium was confined in a 170-$\mu$m-inner-diameter fused silica capillary. The capillary acts as a waveguide for the light [24] and allows for a longer interaction length compared to the confocal parameter. The capillary was held in a V-shaped aluminium groove contained within a vacuum cell. The entire vacuum assembly was mounted on position-adjustment stages in order to aid alignment of the laser beam. It is worth noting at this point that no precautions were taken to recompress the output pulse generated in this experiment to the minimum duration (this could be done employing a pair of prisms or gratings or a spatial-light modulator [25]).

The $\lambda_2$ pulse energy that we used was 60 $\mu$J before the cell window, corresponding to a transmitted energy of approximately 30 $\mu$J measured at the output of the capillary. The $\lambda_1$ pulse energy was reduced to 500 $\mu$J at the capillary entrance, in order not to damage the capillary and not to induce other undesired nonlinear effects such as a Kerr-lensing in the quartz window that could affect the propagation of the $\lambda_2$ pump when the two pulses were overlapping in time. The transmitted energy of the $\lambda_1$ pulse measured at the output of the cell was 120 $\mu$J. We estimate that the intensities of the two beams were $I_1 \sim 1 \times 10^{13}$ W/cm$^2$ and $I_2 \sim 1 \times 10^{12}$ W/cm$^2$ inside the capillary core.

The anti-Stokes spectrum of the generated radiation was measured using a compact fiberoptic spectrometer (Ocean Optics USB2000) with a spectral range from 200 to 850 nm and a calibrated spectral response. The Stokes spectrum could not be measured in this way since it falls outside the spectral range of our spectrometer. Nevertheless, strong generated Stokes sidebands could be seen by dispersing the generated radiation with a prism onto an infrared-sensitive card.

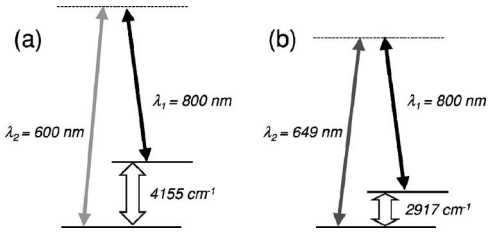


FIG. 4. In every experiment the wavelength $\lambda_2$ of the OPA pulse is tuned in such a way to obtain a condition of Raman resonance. (a) In the case of hydrogen the width of the fundamental vibrational transition is 4155 cm$^{-1}$, hence the OPA wavelength is set to $\lambda_2 = 600$ nm. (b) In the case of methane the width of the fundamental vibrational transition is 2917 cm$^{-1}$, hence the OPA wavelength is set to $\lambda_2 = 649$ nm.

## IV. EXPERIMENTAL RESULTS

We report in this section the results of several measurements of HSRS carried out in methane ($CH_4$) and hydrogen ($H_2$) at different pressures ranging from 100 mbar to 3 bar. When the two input pulses are injected into the gas-filled capillary, multiple Raman sidebands are generated, all in the same direction (i.e., collinear with the capillary axis and with the propagation direction of the input pulses).

For all gas pressures the spectra obtained using the pulse at $\lambda_1$ only (blocking the OPA) were also recorded, in order to show the difference between the two-color and the single-color pumping scheme. It should be noted that, although in both cases most of the pump pulse energy is contained in the $\lambda_1$ pulse, under all the conditions investigated there was no Raman sideband generation using this laser pulse alone.

As shown in the next sections, clear line-broadening effects are present when the highest pulse intensities and gas pressures are used. This prompted us to carry out similar experiments by stretching the $\lambda_1$ pulse, which is the shortest and most intense of the two.

Another set of measurements, which is also reported, was carried out by changing the polarization of the $\lambda_1$ pulse.

### A. Spectra measured with hydrogen at different pressure

Several measurements of the spectra generated using hydrogen as Raman medium were made for different pressures up to the maximum safe value allowed by the cell windows ($p \sim 3$ bar). The relevant transition is the lowest-order vibrational transition, between the ground state ($v=0$) and the first excited vibrational state ($v=1$), whose width is 4155 cm$^{-1}$. In order to obtain the Raman resonance the OPA wavelength was tuned to $\lambda_2 = 600$ nm [Fig. 4(a)].

Figure 5 shows the generated spectra after propagating the two pump pulses through the capillary filled with gas at pressures from 100 mbar up to 3 bar (grey curves). A generated anti-Stokes sideband at $\lambda = 480$ nm is already clearly present for a pressure as low as 100 mbar, and its intensity is of the order of a few percent of the transmitted pulses at the pump frequencies [Fig. 5(a)]. The second anti-Stokes sideband at $\lambda = 400$ nm is generated with a pressure of 500 mbar [Fig.

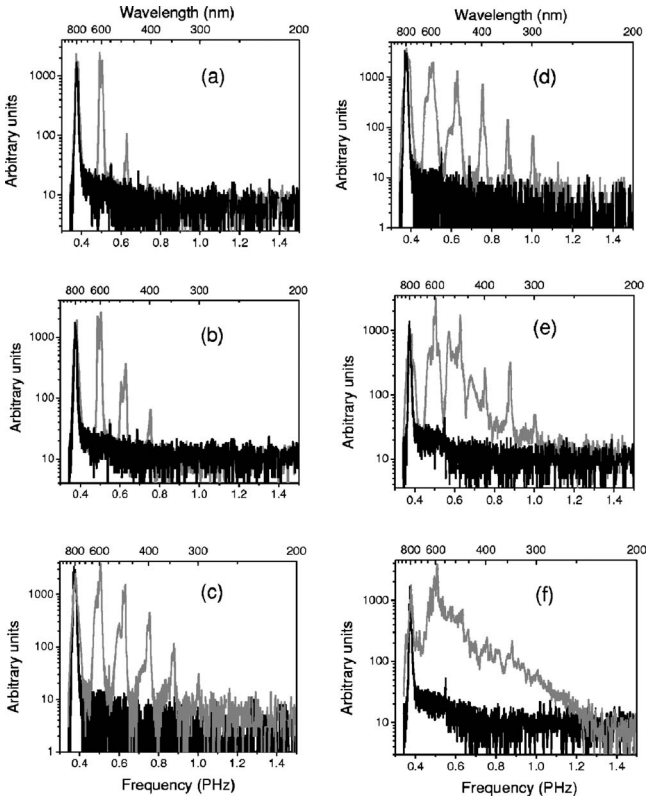


FIG. 5. HSRS spectra generated in hydrogen at different pressures: (a) 100 mbar; (b) 500 mbar; (c) 800 mbar; (d) 900 mbar; (e) 1.7 bar; (f) 3 bar. In each graph the grey curve represents the output spectrum using two input pulses (i.e., the first two lines from the left are the input wavelengths and the other components are Raman sidebands). The black curves represent the output spectra obtained for each gas pressure using only the infrared $\lambda_1$ pump pulse.

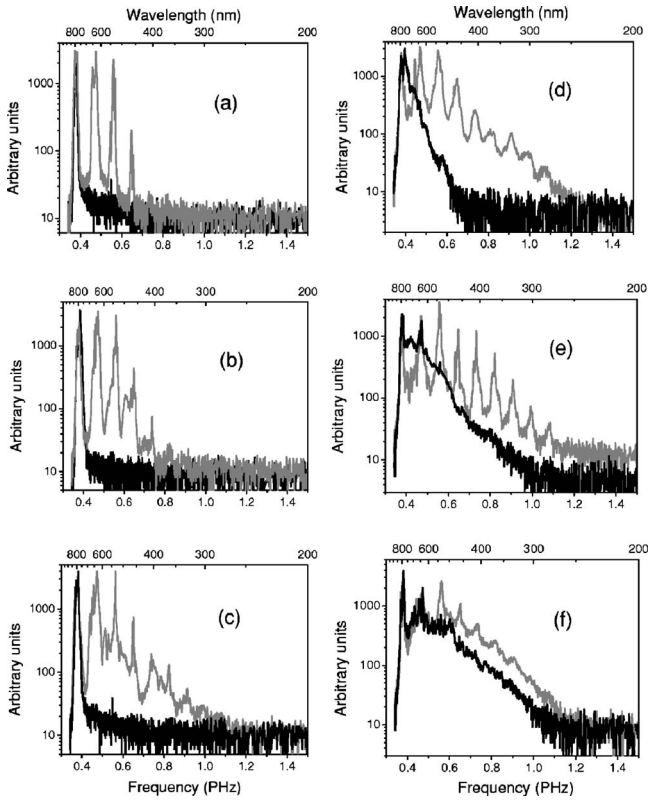


FIG. 6. HSRS spectra generated in methane at different pressures: (a) 300 mbar; (b) 500 mbar; (c) 700 mbar; (d) 900 mbar; (e) 1.6 bar; (f) 3 bar. In each graph the grey curve represents the output spectrum using two input pulses (i.e., the first two lines from the left are the input wavelengths and the other components are Raman sidebands). The black curves represent the output spectra obtained for each gas pressure using only the infrared $\lambda_1$ pump pulse.

5(b)] and the third and fourth sidebands (at wavelengths of 343 and 300 nm, respectively) are visible in the spectrum measured with 800 mbar [Fig. 5(c)]. The numbers of generated sidebands increased up to the fifth anti-Stokes ($\lambda = 267$ nm) at a pressure of 0.9 bar. At this pressure strong pump depletion was observed and up to five anti-Stokes sidebands were observed to have energies exceeding 10% of the transmitted pump pulse energies. We also note that at least one strong sideband was generated on the Stokes side ($\lambda = 1198$ nm) that could be observed by dispersing the generated radiation with a prism onto a piece of IR-sensitive paper.

No Raman sidebands are produced with the single-pulse pumping with any of these pressures, which confirms the importance of the presence of the $\lambda_2$ field at the input for efficient generation of high-order sidebands, as expected.

For pressures of 1.7 bar and higher the number of generated sidebands does not increase. What happens instead is that the sidebands get broadened and the generated spectrum progressively evolve from a comb of a few discrete sidebands to a broad quasicontinuum [Figs. 5(e) and 5(f)].

### B. Spectra measured with methane at different pressure

A similar set of measurements compared to those reported for $H_2$ was made using methane ($CH_4$) as the Raman-active medium. The relevant Raman transition was the same lowest-order vibrational transition as in the case of hydrogen. Swapping between the different gases proved straightforward and required a simple retuning of the OPA wavelength to the relevant Raman resonance. This shows the flexibility of our setup as far as the choice of Raman medium is concerned. In fact, the same experimental setup could be applied to different Raman-active gases, like $D_2$, $CO_2$, $N_2$, NO and many others. For the case of methane the frequency of the fundamental vibrational transition is 2917 $cm^{-1}$, which dictates that the condition of Raman resonance is obtained by setting the OPA output wavelength to $\lambda_2 = 649$ nm [Fig. 4(b)].

Figure 6 shows the generated spectra after propagating the two pump pulses through the capillary filled with gas at pressures ranging from 300 mbar to 3 bar (grey curves). Up to two anti-Stokes sidebands were generated with a pressure as low as 300 mbar [Fig. 6(a), grey curve] and the number of sidebands increased up to as many as 7 with 1.6 bar [Fig. 6(e), grey curve]. Due to the smaller Raman spacing (i.e., longer vibrational period) of methane compared to hydrogen, although more sidebands are generated with methane, in fact in both cases the generated frequency bandwidth is approximately the same. It should be noted that such bandwidth is as broad as the pump frequency value ($\Delta\nu \sim \nu_1$).

The conversion efficiency was remarkably high in this case too, with the first generated anti-Stokes sideband at $\lambda$

=545 nm having an intensity even higher than the pump pulses at the output of the cell and 4 more sidebands having intensities of the order of 10% of the pump intensities (under condition of strong pump depletion) or more. We also note that in the case of methane too at least one strong sideband was generated on the Stokes side ($\lambda \sim 1040$ nm) that could be observed by dispersing the generated radiation with a prism onto a piece of IR-sensitive paper.

As in the case of hydrogen, for pressures higher than 2 bar the number of generated sidebands does not increase further and again what happens is that the sidebands broadens and the generated spectrum gradually evolves towards a broad continuum for a pressure of 3 bar [Fig. 6(e), grey curve].

As with hydrogen, no Raman sidebands are produced with the single-pulse excitation (Fig. 6, black curves), which confirms the importance of the presence of the $\lambda_2$ field at the input for efficient generation of high-order sidebands, as expected. In these single-pump spectra, for pressures of 900 mbar and higher a blueshifted shoulder appears on the infrared pump pulse spectrum. We attribute this effect to self-phase modulation (SPM). In fact, it is a well established technique to employ SPM of short laser pulses in gas-filled hollow fibers in order to achieve spectral broadening for subsequent recompression [24]. A similar effect is not observed in hydrogen due to the fact that its nonlinear coefficient $n_2$ is lower than the one of methane by more than a factor of 4 [26].

This broadening effect is more and more important for higher pressures. As can be seen in Figs. 6(e) and 6(f) the broadening spans over the spectral region of the first 3 or 4 anti-Stokes lines. When this happens it is clearly possible to see weak Raman sidebands superimposed on the quasicontinuous structure. This could be due to the fact that the radiation generated by means of SPM starts stimulating the Raman process, giving rise to the generation of Raman sidebands. The resulting spectrum is therefore the combination of both SPM and SRS.

It is very interesting to see how the presence of the second Raman-resonant $\lambda_2$ pump pulse (the OPA) at the input completely changes the results. It is clear from Fig. 6(e) (grey curve), for example, that when the OPA pulse is present the energy is preferentially channeled to the higher-order sidebands. This is a clear signature of the competition between different nonlinear processes [14], which occurs for strong pump depletion (as it is the case in our experiment).

As already seen, at $p=3$ bar it appears that SPM starts being important even when the second pulse is present [Fig. 6(f), grey curve], although it should be noted that the generated spectrum is still much broader that the single-pump case [Fig. 6(f), black curve—note the logarithmic scale].

### C. Spectra obtained with stretched IR pump pulse

In order to further investigate the nature of this quasicontinuum generation we repeated the experiment, this time stretching (and chirping) the $\lambda_1$ pulse, which is the shortest and by far most intense of the two pump pulses. In order to broaden the pump pulse by an appropriate amount a

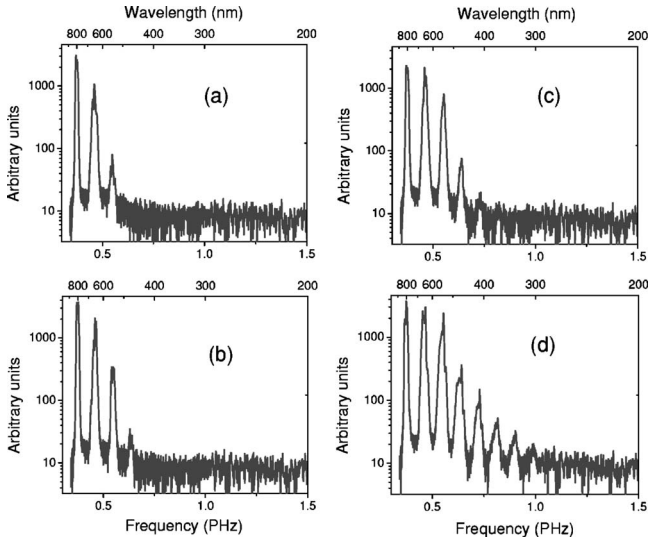


FIG. 7. HSRS spectra generated using two Raman-resonant input pulses in methane at different pressures: (a) 100 mbar; (b) 300 mbar; (c) 600 mbar; (d) 900 mbar. Differently from Fig. 6, the $\lambda_1$ pump pulse was stretched from $\tau \simeq 100$ fs to $\tau \simeq 400$ fs by propagating it through a 20-cm-long fused silica block.

20-cm-long silica rod that was available was employed. After propagation through the rod the pulse duration was stretched from $\tau_1 \simeq 100$ fs to $\tau_1 \simeq 400$ fs. All the other parameters (pulse energies and $\lambda_2$ pulse duration) were left unchanged compared to the results of the previous section.

The anti-Stokes spectra generated in this configuration are shown in Fig. 7 for different pressures up to 900 mbar. We can see that many anti-Stokes sidebands are efficiently generated, with an efficiency comparable to the case of shorter $\lambda_1$ pump pulse ($\tau_1 \simeq 100$ fs, see Fig. 6). In this case the generated sidebands do not appear to be affected by any spectral broadening, as was the case before. This is even more evident in Fig. 8(b), where the spectrum generated with a gas pressure of 3 bar is shown. The result obtained with the same pressure and shorter $\lambda_1$ pulse ($\tau_1 \simeq 100$ fs) is also shown

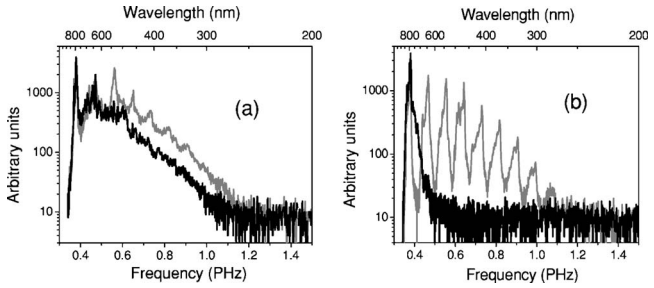


FIG. 8. HSRS spectra generated in methane at a pressure of 3 bar. In each graph the the grey curve represents the output spectrum using two input pulses, i.e., the first two lines from the left are the input wavelengths and the other components are Raman sidebands, whereas the black curves represent the output spectra obtained for each gas pressure using only the infrared $\lambda_1$ pump pulse only. (a) Output spectra using a short $\lambda_1$ pulse ($\tau_1 \simeq 100$ fs), same as in Fig. 6(f). (b) Output spectra using a longer $\lambda_1$ pulse ($\tau_1 \simeq 400$ fs).

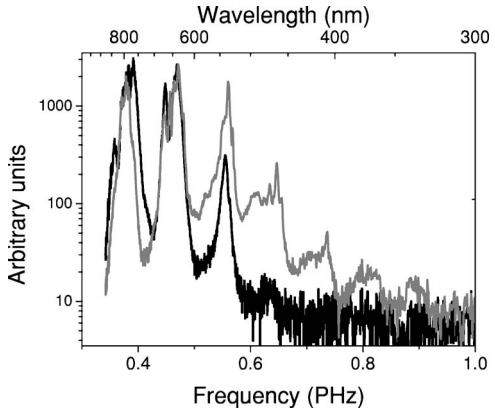


FIG. 9. HSRS spectra generated using two linearly polarized input pulses, either parallel (grey curve) or perpendicular (black curve) to each other.

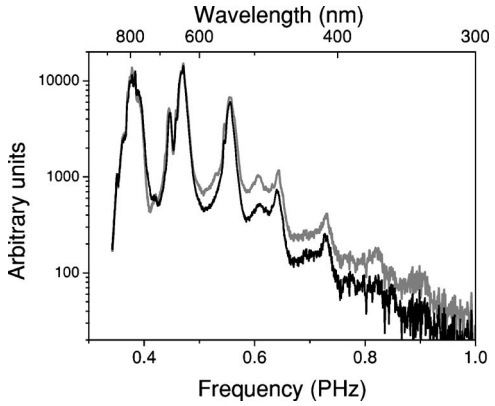


FIG. 10. HSRS spectra generated after changing to circular the polarization of the $\lambda_1$ input pulse, while keeping the polarization of the $\lambda_2$ pulse linear (black curve), compared to the case of both polarizations linear and parallel to each other (grey curve).

again in Fig. 8(a) for comparison. It is evident the different broadening of the generated spectrum, which is essentially continuum with the shorter $\lambda_1$ pump pulse whereas it is constituted by a comb of well-defined sidebands with the longer $\lambda_1$ pulse. The overall spectral extent of the generated spectrum is approximately the same in the two cases.

The output spectrum obtained with the $\lambda_1$ pulse only is also shown in Fig. 8 without the $\lambda_2$ pulse for both values of $\tau_1$. The spectral broadening is almost negligible in the case of longer pulse duration compared to the case of shorter duration. This findings seems to suggest that indeed SPM, whose effect decreases for longer pulse duration (lower intensity gradients), plays a determinant role in the observed spectral broadening.

### D. Polarization-dependence results

We have also examined the dependence of the efficiency of the Raman sidebands generation process upon the polarization of the laser field. The configuration previously described (with the two polarizations being linear and parallel to each other) is expected to be the most effective and this is what we sought to verify experimentally.

We changed the polarization of the Ti:sapphire laser fundamental wavelength $\lambda_1 = 800$ nm, while the polarization of the OPA pulse at $\lambda_2$ nm remains the same (i.e., linear). The experimental setup is thus the same as before, with the only exception of either a half-wave plate or a quarter-wave plate in the path of the 800 nm beam to change its polarization to linear and rotated by 90° or circular, respectively. The pulse durations were set at their minima ($\tau_1 \simeq 100$ fs and $\tau_2 \simeq 250$ fs), without any additional stretching factor as in Sec. IV C. The Raman medium was methane at a pressure of 500 mbar.

Figure 9 shows the spectra obtained employing two linearly polarized laser pulses, parallel to each other in one case (grey curve) and perpendicular in the other case (black curve). It is clearly evident that the Raman generation is maximal for the case of parallel polarizations. For perpendicular polarizations the intensity of the generated sidebands is strongly reduced (by an order of magnitude). It is also evident that the spectral broadening of the $\lambda_1$ pulse is more pronounced in the case of perpendicular polarization (black curve) compared to the other case. This again shows how a reduced Raman generation is accompanied by a larger degree of line broadening through self-phase modulation, exactly as we saw in the measurement reported in the previous section.

Figure 10 shows the spectrum obtained after changing the polarization of the $\lambda_1$ pulse to circular (black curve). Compared to the case of linear and parallel polarizations (grey curve) the Raman generation is again slightly reduced, although by a much smaller factor compared to the case of linear and perpendicular polarizations. The circular polarization is the sum of two dephased orthogonal linear polarizations, therefore the resulting intensity must be expected to be in between the intensities of the two linear-linear experiments. The use of two circular polarization might be more interesting in order to give information on the symmetry of the electronic transitions. This measurement was not carried out in the present experiment as a suitable quarter-wave-plate for the pump pulse at $\lambda_2$ was not available at the time of the experiment.

## V. NUMERICAL SIMULATION AND COMPARISON WITH THE EXPERIMENTAL RESULTS

We obtain important insights by comparing the numerically predicted Raman spectra at a given interaction length with the experimental data. One such predicted spectrum is shown in Fig. 11, which is taken at 40 cm for parameters that match the experimental data in Fig. 5(d). We see that there is good agreement, both in the number of sidebands generated on both the Stokes and anti-Stokes sides, and also in terms of the energy conversion efficiency. This agreement gives us confidence that our theoretical model constitutes a reliable tool to interpret and explain the experimental results, and also to extract information about quantities that are not directly accessible through experimental measurements.

The broader spectral widths of the experimentally measured Raman lines compared to the predicted lines can be attributed to self-phase modulation, which is always present

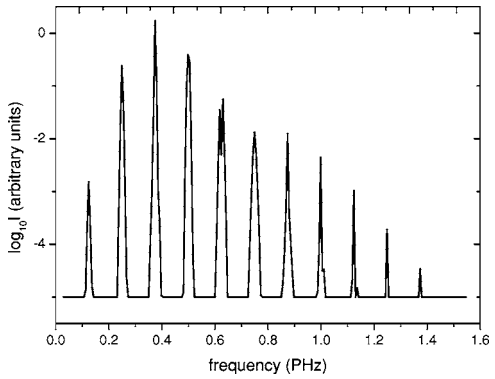


FIG. 11. Calculated Raman spectrum after a propagation length $z=40$ cm and with pulse intensities as in Fig. 12. The input frequencies are the lines at 0.375 PHz ($\lambda_1=800$ nm) and 0.5 PHz ($\lambda_2=600$ nm).

to a certain degree in the experimental data but is neglected in the calculation. In addition, the experimental pump pulses are slightly chirped (particularly the $\lambda_2$ pulse, due to the amount of material along the OPA path), whereas the numerical model uses unchirped pulses with the same duration of the experiment.

One significant advantage of a reliable numerical model is that we can easily see properties of the experimental system which are hidden from experimental view. For example, with our current setup where we confine the Raman medium using a capillary, it is not possible to see how the sidebands develop as a function of interaction distance. We might try to do this by changing the gas pressure, but then the polarization decay of the Raman transition would also change, and so the comparisons would be flawed.

Numerically, however, it is easy to extract such information. For example, Fig. 12 shows the Raman spectrum as a function of both frequency and interaction distance for the same parameters as in Fig. 5(d). The growth of Raman sidebands up to several higher-orders is reproduced. The figure also shows that while the sidebands generally do grow stronger with distance, there can be some decrease or oscillatory behavior. We also see a "saturation" behavior, where the initial strong sideband growth flattens off.

There is no way in the experiments of directly probing the polarization of the Raman transition. Again, this is trivial to

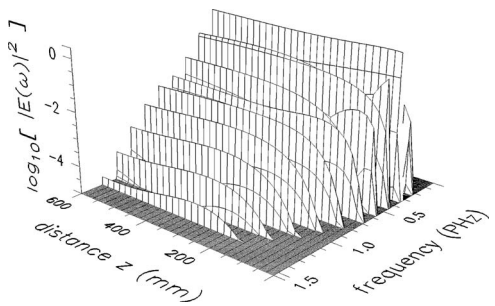


FIG. 12. 3D plot of the calculated Raman sidebands intensity as a function of the frequency and the propagation distance for pump pulse intensities of $I_1=1.5\times10^{13}$ W cm$^{-2}$ and $I_2=1.5\times10^{12}$ W cm$^{-2}$.

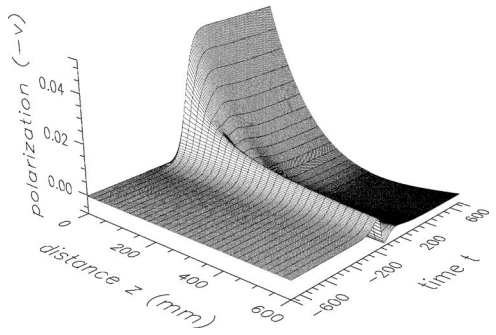


FIG. 13. 3D plot of the polarization $v$ of the medium calculated as a function of time and propagation distance (note that the orientation of the distance axis is reversed with respect to Fig. 12).

extract from our numerical simulations. The polarization $v$ of the medium for the same simulation as in Fig. 12 is shown in Fig. 13 (but note the reversed distance scale). We see that the polarization reaches its highest value ($v\approx0.04$) for short propagation distances and decreases thereafter. This occurs because while the input laser pulse induce a substantial polarization in the medium at early stages of the interaction, at later stages the field also contains increasingly strong Raman sidebands which tend to inhibit the generation of new polarization. An oscillating behavior is also predicted for the final (long time) value of polarization as a function of distance. This behavior can be associated with a similar behavior in the relative strengths of the generated sidebands (Fig. 12).

Possibly the most important insight provided by all the simulations is that a substantial polarization can be generated even at short interaction distances—even though the conditions do not strictly correspond to those reported in the literature for either adiabatic or impulsive preparation of the Raman medium. This has obvious implications for the improvement of our experimental systems.

Another interesting result emerges from the simulation when higher values of the pulse intensities are used (as far as the simulation is concerned, this has a roughly similar effect to a higher gas density). Here, at the longest propagation distances, the Raman spectrum starts to look less like a neat comb of discrete sidebands, but broadens significantly, and appears to evolve towards a quasicontinuum. This result qualitatively reproduces what was observed experimentally at the highest gas density [Fig. 5(f)]. This indicates that the superbroadening effect observed in the experiment at the highest gas density might not be due entirely to self-phase modulation, as this is not considered in the numerical simulations. Further analysis of the details of this superbroadening are at present time under investigation.

Of course, if instead we seed the simulation with only a single pump pulse, the Raman transition is barely excited, and no significant sidebands are generate. This too is in agreement with our experimental observations.

## VI. DISCUSSION

### A. Sideband generation

The most important result that emerges from the experiments is that the generation of spectral sidebands via stimu-

lated Raman scattering with femtosecond pulses is dramatically enhanced by the presence of a second pulse in Raman resonance with the molecular vibrational transition. These results are reproduced by the numerical simulation in terms of number of generated sidebands and energy conversion efficiency.

It should be pointed out that all these results were obtained with pump energies which are considerably lower than previously reported values for SRS threshold with femtosecond pulses [15,16,27] and with much higher conversion efficiency into high-order sidebands.

One factor that limits the conversion efficiency in any single-color scheme is the presence of other nonlinear effects such as self-phase modulation that compete with the Raman process and reduce the raman gain [14]. This effect is clearly evident in all our measurements carried out with one pump pulse only, where spectral broadening effects are clearly present and get larger with increasing gas pressure.

The "competition" between nonlinear effects is shown particularly well in the comparison between spectra obtained with one and two pump pulses for the same conditions, as in the case of Fig. 6(e) (methane at 1.6 bar). It is very evident how the spectrum obtained with the $\lambda_1$ pulse only results in a blueshifted shoulder on the spectrum of the pump pulse and no sidebands being generated. With the same conditions and the additional pump pulse at $\lambda_2$ present the broadening effect disappears and a broadband set of discrete sidebands is generated instead. This indicates that the two-color pumping ensures that the Raman conversion dominates over the competing SPM and the energy is efficiently transferred to the HSRS sidebands.

### B. Spectral "superbroadening" effects

Another feature of interest that has emerged from these experiments is the extremely large extent of the spectral broadening effect that was observed in some cases. In particular, in the case of the highest gas pressure used ($p=3$ bar) and two-pulse pumping the resulting spectrum turned out to be quasicontinuous, spanning from the infrared to the UV [Fig. 6(f)]. As already stated in Sec. IV B we attribute this broadening effect to self-phase modulation. This is consistent with the observed reduction of this effect when longer pump pulses are employed (Sec. IV C) and also with the observation that the broadening of the pump-pulse in the case single-color excitation is much stronger (by a factor 4) for methane than for hydrogen [26]. However, it should be noted that an alternative purely Raman broadening effect appears in the numerical simulation for increasing pulse intensities. This indicates that other mechanisms than SPM could play a role, as already discussed in Sec. V.

### C. Ultrashort pulse synthesis

Radiation constituted by a comb of discrete spectral components can be compressed to a *train* of ultrashort pulses, according to Fourier theory. On the other hand this more continuous spectral structure that we observed holds the potential to be compressed to an *isolated* ultrashort pulse, which could be still more useful for many applications.

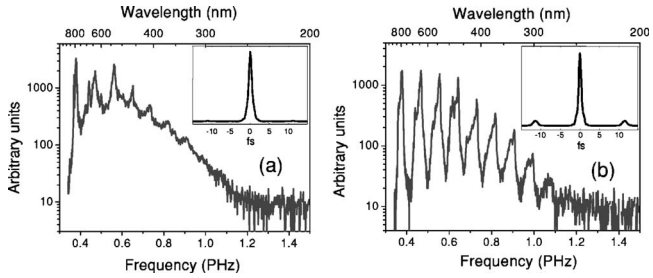


FIG. 14. HSRS spectra obtained with both pump pulses (grey curves) in both cases of (a) shorter ($\tau_1 \simeq 100$ fs) and (b) longer ($\tau_1 \simeq 400$ fs) $\lambda_1$ pump pulses. The insets show the corresponding Fourier transforms (pulse intensity as a function of time). Case (a): an isolated pulse with a full width at half maximum (FWHM) duration of $\tau \simeq 1.0$ fs would be supported, with satellite pulses having an intensity smaller than 1% of the main peak. Case (b): as a consequence of the modulation of the spectrum one gets a temporal structure which is more similar to a pulse train, with a strong main pulse and satellite pulses separated from the main one by a time equivalent to the vibrational period $\tau = 12$ fs; the satellite pulses have intensities of the order of 10% of the main pulse. The FWHM duration of the main pulse is $\tau \simeq 0.82$ fs.

In order to evaluate the potential of the HRSR spectra that we are able to obtain in terms of generation of ultrashort pulses, we performed Fourier transforms of some of these spectra. As we have no information about the properties of the spectral phase, we assume a "flat" spectral phase profile. This corresponds to the ideal case of being able to perfectly compensate every phase distortion across the utilized spectrum. Figure 14 shows the HSRS spectra obtained with both pump pulses (grey curves) in both cases of (a) shorter ($\tau_1 \simeq 100$ fs) and (b) longer ($\tau_1 \simeq 400$ fs) $\lambda_1$ pump pulse duration and the insets show the corresponding Fourier transforms. In the first case (a) the result is that an isolated pulse with a full width at half maximum (FWHM) duration of $\tau \simeq 1.0$ fs would be supported, with satellite pulses having an intensity smaller than 1% of the main peak. In the second case (b) the result is similar but as a consequence of the modulation of the spectrum (more discrete sidebands) one gets a temporal structure which is more similar to a pulse train, with a strong main pulse and satellite pulses separated from the main one by a time equivalent to the vibrational period $T_v = 12$ fs. The satellite pulses have intensities approaching 10% of the main pulse. The FWHM duration of the main pulse is $\tau \simeq 0.82$ fs.

### D. Generated molecular coherence

The high efficiency of the nonlinear Raman conversion means that we are able to excite a substantial molecular coherence in the system, despite the fact that we are using pulses that do not satisfy either the requirements for adiabatic preparation of the sample nor those for impulsive preparation. In fact, our numerical simulation predicts a value of the medium polarization ($\sim v$) of the order of $\sim 4\%$ of the maximal value. This result is obtained for a set of parameters corresponding to those of the experimental situation. Also, these parameters are those that allow a qualita-

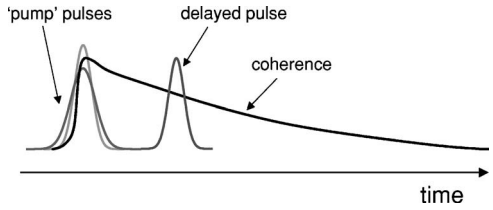


FIG. 15. Scheme of Raman scattering of a delayed pulse over the molecular coherence generated by two Raman-resonant resonant pump pulses.

tive and quantitative reproduction of the Raman sidebands that are generated experimentally.

Since our pump pulses are shorter than the dephasing time $T_2$ (tens of picoseconds regime), the excitation wave in the medium will last after the pump pulses are gone. This offers the opportunity to exploit the coherent molecular motion for subsequent Raman scattering of a delayed probe pulse (possibly a fraction of the same laser that produces the two-color pumping) to generate sidebands in a linear regime, as in the reported impulsive experiments [5]. The probe pulse would be modulated by the oscillating refractive index upon propagation through the coherently excited medium and sidebands generation would occur in a linear and controllable fashion (Fig. 15). This would constitute an alternative solution to obtain phase-locked sidebands.

Compared to an impulsive scheme, our solution has the advantage that it enables one to excite high-frequency Raman transition without any stringent requirements on the pump pulse duration. For example, by efficiently creating a vibrational excitation in hydrogen ($\sim 10^{14}$ Hz)) only three generated sidebands would be enough to synthesize sub-fs pulses [5]. The use of relatively longer pulses with respect to an impulsive single-pump excitation (hundreds of femtoseconds rather than few femtoseconds) would also reduce the effect of competing nonlinear processes on the excitation efficiency. A subfemtosecond pulse generation scheme looks then accessible starting from a single $\sim 100$ fs source, employing the excitation of any desired vibrational motion (even those with the highest frequency, e.g., $H_2$).

Moreover an advantage of this type of scheme using pairs of $\sim 100$ fs laser pulses over the impulsive case is that there is greater selectivity over which vibrational modes are excited. In the impulsive limit the large bandwidth of the laser can lead to simultaneous excitation of other molecular vibrational modes at different frequencies; since these will not be in general of commensurate frequencies, the modulated spectrum will have complex phase relationships between the sidebands that can inhibit recompression.

## VII. CONCLUSIONS

In summary, in this paper a novel scheme for the generation of high-order Raman sidebands and the excitation of coherent molecular vibrations in a highly-transient regime with two-color pumping was investigated numerically and experimentally.

The experimental results obtained have shown high conversion efficiency of the pump energy to a set of Raman sidebands spanning a very broad spectrum, from the infrared ($\lambda > 1$ $\mu$m) to the ultraviolet ($\lambda \sim 260$ nm). This conversion efficiency to HSRS sidebands is higher than those reported in other experiments of highly-transient SRS, where higher gas pressures but only one ultrashort laser pulse instead of two Raman-resonant pulses had been used. The Raman spectra have been measured for hydrogen and methane and the differences between the spectra obtained with the two gases have been explained in terms of self-phase modulation.

The experimental results are well reproduced by numerical simulations based on a semiclassical model, where the field is treated classically and the medium is treated quantum-mechanically. These simulations are able to reproduce with good accuracy the experimental result as far as the efficient generation of high-order SRS sidebands is concerned. They also qualitatively reproduce the superbroadening effect that was experimentally observed at the highest gas density.

The simulation allows us to deduce values for the degree of material excitation and to make explicit predictions about the spatio-temporal evolution of the coherence (i.e., medium polarization, $\sim v$) generated in the medium. Such coherence can reach a value of the order of $\sim 4\%$ of the maximal value.

These results are significant for several reason. First of all, the ultrabroadband pulses obtained could allow the generation of extremely short pulses (down to the subfemtosecond limit) if it is possible to precisely characterize and compensate any distortions of the spectral-phase profile. Furthermore, the substantial degree of molecular coherence that can be created in the system could permit other SRS schemes to be implemented, where a delayed pulse scatters off the generated coherence. These results provide an improved understanding of the characteristics of HSRS pumped by femtosecond laser pulses and pave the way towards the demonstration of a source of energetic radiation in the subfemtosecond regime of pulse duration.

## ACKNOWLEDGMENTS

We gratefully acknowledge the contributions of J.S. Robinson and N. Hay, useful discussions with R. Velotta, M. Anscombe, and S. Gundry and the technical support of P. Ruthven and A. Gregory. This work was supported by the UK EPSRC and by the European research training network COCOMO (Contract No. EU-IHP HPRN-CT-1999-0129.

[1] N. A. Papadogiannis, B. Witzel, C. Kalpouzos, and D. Charalambidis, Phys. Rev. Lett. **83**, 4289 (1999).
[2] P. M. Paul, E. S. Toma, P. Breger, G. Mullot, F. Auge, P. Balcou, H. G. Muller, and P. Agostini, Science **292**, 1689 (2001).
[3] M. Hentschel, R. Kienberger, C. Spielmann, G. A. Reider, N. Milosevic, T. Brabec, P. Corkum, U. Heinzmann, M. Drescher, and F. Krausz, Nature (London) **414**, 509 (2001).
[4] S. E. Harris and A. V. Sokolov, Phys. Rev. Lett. **81**, 2894 (1998).
[5] A. Nazarkin, G. Korn, M. Wittmann, and T. Elsaesser, Phys. Rev. Lett. **83**, 2560 (1999).
[6] E. Sali, K. J. Mendham, J. W. G. Tisch, T. Halfmann, and J. P. Marangos, Opt. Lett. **29**, 495 (2004).
[7] Y. R. Shen, *The Principles of Nonlinear Optics* (Wiley, New York, 1984).
[8] Y. X. Yan, E. B. Gamble, and K. A. Nelson, J. Chem. Phys. **83**, 5391 (1985).
[9] A. V. Sokolov, D. R. Walker, D. D. Yavuz, G. Y. Yin, and S. E. Harris, Phys. Rev. Lett. **85**, 562 (2000).
[10] D. D. Yavuz, D. R. Walker, G. Y. Yin, and S. E. Harris, Opt. Lett. **27**, 769 (2001).
[11] A. V. Sokolov, D. R. Walker, D. D. Yavuz, G. Y. Yin, and S. E. Harris, Phys. Rev. Lett. **87**, 033402 (2001).
[12] A. Nazarkin and G. Korn, Phys. Rev. A **58**, R61 (1998).
[13] A. Nazarkin, G. Korn, and T. Elsaesser, Opt. Commun. **203**, 403 (2002).
[14] I. G. Koprinkov, A. Suda, P. Wang, and K. Midorikawa, Opt. Commun. **174**, 299 (2000).
[15] V. Krylov, O. Ollikainen, U. P. Wild, A. Rebane, V. G. Bespalov, and D. I. Staselko, J. Opt. Soc. Am. B **15**, 2910 (1998).
[16] I. G. Koprinkov, A. Suda, P. Wang, and K. Midorikawa, Opt. Lett. **24**, 1308 (1999).
[17] L. L. Losev, A. P. Lutsenko, and S. P. Azonov, Sov. J. Quantum Electron. **20**, 878 (1990).
[18] T. Imasaka, S. Kawasaki, and N. Ishibashi, Appl. Phys. B: Photophys. Laser Chem. **49**, 389 (1989).
[19] A. E. Dangor, A. K. L. Dymoke-Bradshaw, A. Dyson, T. Garvey, S. J. Kerttunen, J. P. Partanen, R. R. E. Salomaa, A. J. Cole, C. Danson, C. B. Edwards *et al.*, J. Phys. B **22**, 797 (1989).
[20] L. L. Losev, J. Song, J. F. Xia, D. Strickland, and V. V. Brukhanov, Opt. Lett. **27**, 2100 (2002).
[21] A. P. Hickman, J. A. Paisner, and W. K. Bischel, Phys. Rev. A **33**, 1788 (1986).
[22] K. S. Syed, G. S. McDonald, and G. H. C. New, J. Opt. Soc. Am. B **17**, 1366 (2000).
[23] P. Kinsler and G. H. C. New, Phys. Rev. A (in press).
[24] M. Nisoli, S. D. Silvestri, and O. Svelto, Appl. Phys. Lett. **68**, 2793 (1996).
[25] T. Baumert, T. Brixner, V. Seyfried, M. Strehle, and G. Gerber, Appl. Phys. B: Lasers Opt. **65**, 779 (1997).
[26] R. L. Sutherland, *Handbook of Nonlinear Optics* (Marcel Dekker, New York, 2003).
[27] V. Krylov, A. Rebane, D. Erni, O. Ollikainen, U. Wild, V. Bespalov, and D. Staselko, Opt. Lett. **21**, 2005 (1996).